A Three-Port Hybrid-Bridge Based Bidirectional Series-Resonant Converter with Wide Voltage Conversion Gain

Jiahui Wu[1], Dong Liu[2*], Yanbo Wang[1], Thiago Pereira[3], Marco Liserre[3], Zhe Chen[1]
[1]Department of Energy Technology, Aalborg University, Aalborg, Denmark
[2]Group of Power Electronics, Lightyear, Helmond, Netherland
[3]Chair of Power Electronics, Kiel University, Kiel, Germany
Corresponding author (Email) *: liudong@ieee.org

***Abstract*— A novel three-port hybrid-bridge based bidirectional series-resonant converter with the corresponding modulation strategy is proposed. The proposed converter consists of a three-level (3L) full bridge and two two-level (2L) full bridges can be utilized for interfacing the medium voltage and low voltage DC grids. The first-harmonic-synchronized PWM (FHS-PWM) control plus phase-shift control are used for the proposed converter to obtain four degrees of control freedom and a wide range of voltage conversion gain. Zero-voltage switching (ZVS) of all power switches can be achieved within the entire operating range due to the series-resonant tanks. Besides, the voltage gain of the proposed converter is only determined by the duty cycles and independent of the load (i.e. as DC transformer). The operational principle and characteristics of the proposed converter are analyzed. Finally, simulation results are provided to verify the proposed converter.**

***Index Terms*—First-harmonic-synchronized PWM (FHS-PWM), four degrees of control freedom, hybrid bridge, three-port convertor**

I. INTRODUCTION

With the increasing utilizations of renewable energy source such as photovoltaic and wind turbines in the energy system, there exist intermittent and unstable issues introduced by renewable energy source. Integration with energy storage system (ESS) have become an attractive choice [1-3]. And the three-port converter (TPC) has been widely studied for improving the performance of ESS integration.

Normally, TPC can be classified into unidirectional converter and bidirectional converter. For unidirectional converter, no more than two ports can be interchanged in input and output mode. Reference [4] proposes a novel TPC composed of an asymmetric three-level (A3L) full bridge in primary-side and uncontrolled rectifier bridge in secondary-side to interface the photovoltaic (PV) generation with battery. And the battery port is connected to the neutral-points and bidirectional operates to balance the load requirement and PV generation. With the similar application, reference [5] proposes a hybrid-connected TPC with a full bridge in primary-side and an asymmetric full-bridge in secondary-side to reduce the peak and root-mean-square (RMS) current values and circulating conduction losses. To obtain compact structure, reference [6] proposes a new non-isolated TPC with reduced component count by developing different power flow graphs and selecting the most appropriate converters arrangement. For bidirectional TPC derived from the dual-active-bridge (DAB) topology [7] is more suitable for power flow management thanks to the interchange ability of input and output mode for all ports. Reference [8] proposed a dual transformer based TPC with self-current sharing structure, high power density and decoupled power flow management can be obtained.

Besides, soft switching technology with resonant device is also a good candidate for improving the efficiency of TPC. In [9], a three-port LLC resonant converter with A3L full-bridge is proposed to achieve high power density thanks to fewer power device. But part of the converter is bidirectional and isolated. To solve the magnetic bias issue, [10] proposes a series resonant hybrid-bridge-based TPC converter with dual half bridges plus one full bridge, and the decoupling between the other two ports can be achieved by setting the resonant frequency of one of the three ports equal to the switching frequency. In terms of control strategy, traditional PWM control with fix switching frequency is proposed for resonant TPC converter in [11], but the voltage gain is coupled with the load. To solve this issue, [12] propose a first-harmonic-synchronized (FHS) PWM control in DAB converter, the voltage gain is only determined by the effective duty cycle and has nothing to do with the amplitude and direction of the transferred power. Based on [12], [13] utilized the FHS PWM control in TPC converter. However, the voltage conversion gains of TPC under these control strategies are only adjusted by single variable, thus wide range of voltage gain may be not satisfied.

Based on the above context, this paper proposes a novel three-port hybrid-bridge based bidirectional series-resonant converter with corresponding control strategy for interfacing between the medium voltage DC (MVDC) and low voltage DC (LVDC). The features as follows can be achieved for the proposed converter.

1) The voltage stress of power switches in port 1can be reduced by half due to the three-level (3L) structure.

2) Wide voltage gain can be obtained thanks to four degrees of control freedom.

3) The voltage gain is only determined by the duty cycles of power switches and independent of the transferred power.

4) ZVS of all power switches can be achieved.

The circuit topology and operation principle are introduced in Section II, the analysis of the characteristics and performances of the proposed converter is carried out in Section III, followed by a simulation verification of the correctness of the proposed converter in Section IV. A brief conclusion is given in Section V.

II. Circuit Topology and Operation Priciple

A. Circuit Topology

Fig. 1 shows the circuit topology of the proposed converter, which is consisted of a neutral-point-clamped (NPC) type 3L full bridge, two two-level (2L) full bridges, two series-resonant tanks, two auxiliary inductors, and a high frequency three-winding transformer. Port 1 with 3L structure is connected to MVDC, Port 2 and Port 3 with 2L structure are connected to LVDC. V_1, V_2 and V_3 are the voltages of port 1, port 2 and port 3 respectively. The turns ratio of transformer is n_1: n_2: n_3. And the resonant inductors and capacitors of the two resonant tanks are the same, namely, L_{r1}=L_{r2}=L_r, C_{r1}=C_{r2}=C_r. The voltage of port 1 is split into V_{cs1} and V_{cs2} halves of V_1 by C_{s1} and C_{s2}. It should be mentioned that the two auxiliary inductors are utilized to improve the zero-voltage-switching (ZVS) characteristics of the converter, but don't resonant with the resonant tanks, which are equal to the equivalent magnetic inductor of the transformer, namely, L_{a1}=L_{a2}=L_m/n^2.

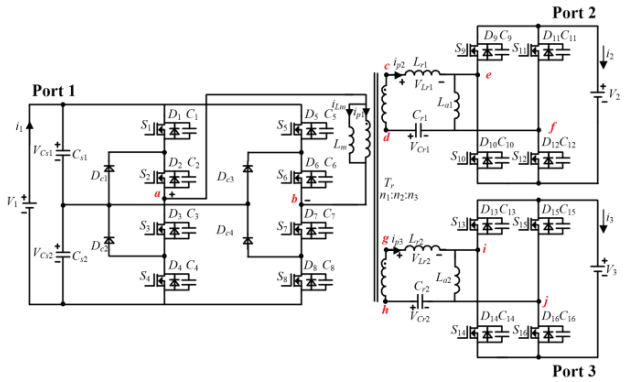

Fig.1 Circuit topology of proposed converter

The switching frequency is constant as resonant frequency of each resonant tank, which can be expressed as (1).

$$f_s = \frac{1}{2 \cdot \pi \sqrt{L_r \cdot C_r}} \tag{1}$$

Where f_s is the switching frequency.

B. Operation Principle

The first-harmonic-synchronized PWM (FHS-PWM) control plus phase-shift (PS) control are utilized for the proposed converter, which can operate not only in single input double outputs (SIDO) mode, but also double inputs single output (DISO) mode. And the operation principle of these two working modes is the same.

Take the SIDO mode an example to illustrate the operation principle of the proposed converter with the corresponding modulation strategy, which is presented as Fig. 2. In Fig. 2, Port 1 is the input port, Port 2 and Port 3 are output ports. T_s is the switching period. D_1 is the duty cycle of power switches S_1, S_4, S_5, and S_8 in port 1, S_2, S_3, S_6, and S_7 conduct complementarily. D_2 is the duty cycle of phase shift delay between the two legs in port 1. D_3 and D_4 are the duty cycles of S_9, S_{11} and S_{13}, S_{15} in port 2 and port 3, respectively. The other power switches of port 2 and port 3 also conduct complementarily. V_{ab}, V_{cd}, and V_{gh} present the midpoint voltages of the bridges in port 1, port 2, and port 3. i_{p1}, i_{p2}, and i_{p3} present the currents through the three windings of transformer.

From Fig. 2, it can be seen that 1) the midpoint voltage of Port 1 V_{ab} is symmetrical in each half of switching period and has five level voltage levels in total, i.e., -V_1, -V_1/2, 0, V_1/2, V_1. And two degrees of control freedom including the D_1 and D_2 can be used to adjust the length of the five level voltage levels in port 1; 2) the midpoint voltage of Port 2 V_{cd} is centrosymmetric to V_{ab}, which has three level voltage levels in total, i.e., -V_2, 0, V_2, the case of the midpoint voltage of Port 3 V_{gh} is the same as V_{cd}; 3) the length of voltage levels of V_{cd} and V_{gh} can be adjusted by D_3 and D_4, respectively. As a result, the proposed converter with the corresponding control strategy has four degrees of control freedom, wide voltage gain can be obtained comparing with the existed TPC.

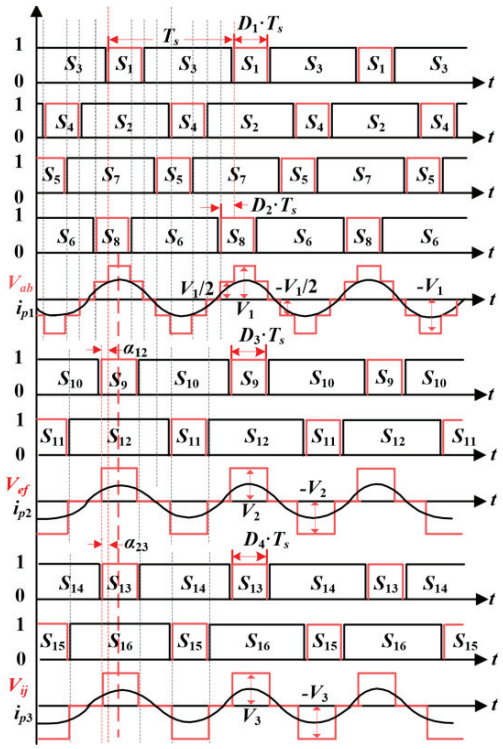

Fig. 2 Operation principle of proposed converter

It should be mentioned that the constraints D_1>D_2 and D_1+D_2≤1 should be satisfied to make sure V_{ab} has five level voltage levels. Besides, to keep the fundamental component of the midpoint voltages V_{ab}, V_{cd}, and V_{gh} in synchronized, the phase shift angles between each port should be set as (2).

$$\begin{cases} \alpha_{12} = \dfrac{D_3 - D_1 + D_2}{2} \cdot T_s \\ \alpha_{13} = \dfrac{D_4 - D_1 + D_2}{2} \cdot T_s \end{cases} \tag{2}$$

Where α_{12} is the phase shift angle between Port 1 and Port 2, α_{13} is that of between Port 1 and Port 3. From (2), it can be seen that α_{12} and α_{13} are dependent on D_1, D_2, D_3, and D_4.

III. Characteristics and Performances

A. Voltage Gain

Before deriving the voltage gain, the equivalent circuit of the proposed hybrid-bridge-based TPC is shown in Fig. 3.

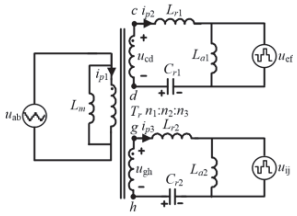

Fig. 3 Equivalent circuit of proposed converter

In Fig. 3, the auxiliary inductors and magnetizing inductance of the transformer can be ignored thanks to the directly connection to the middle point of the bridges in Port 1, Port 2, and Port 3. Besides, the impedances of the two resonant tanks are equal to zero when the proposed converter always operates in resonant frequency point, thus the voltages of the transformer in port 2 and port 3 are equal to the middle point voltages u_{ef} and u_{ij} including the fundamental components which are presented as

$$\begin{cases} u_{ef1} = u_{cd1} \\ u_{ij1} = u_{gh1} \end{cases} \tag{3}$$

where u_{ef1}, u_{cd1}, u_{ij1}, and u_{gh1} are the fundamental components of u_{ef}, u_{cd}, u_{ij}, and u_{gh}, respectively.

The main operation waveforms of the proposed converter with the corresponding modulation strategy are presented as Fig. 4, where Fig. 4(a) is the waveforms of the SIDO mode, i.e., Port 1 is the input port, Port 2 and 3 are the output ports, while Fig. 4(b) is the waveforms of the DISO mode, i.e., Port 1 is the out port, Port 2 and 3 are input ports. And the values of t_1-t_7 within half switching period are listed in Table I.

According to Fig. 4, it can be seen that the operation principles of SIDO mode and DISO mode are the same except that the resonant currents of each port are reversed. Besides, the middle point voltages V_{ab}, V_{ef}, and V_{ij} are in synchronized by setting the phase shift angles between each port as (2), and D_3 is equal to D_4 when the turns ratio of transformer n_2: n_3=1:1, thus making the fundamental components of V_{ab}, V_{cd}, and V_{gh} are the same in both magnitude and phase. It has

$$u_{ab1} = u_{cd1} = u_{gh1} \tag{4}$$

Where V_{ab1} is the fundamental components of V_{ab}. Based on the first harmonic approximation (FHA) method [14], V_{ab1}, V_{ef1} and V_{ij1} can be obtained as:

$$V_{ab1} = \frac{4V_1}{\pi}\sin(\pi D_1)\cos(\pi D_2)e^{i\frac{\pi}{2}} \tag{5}$$

$$V_{ef1} = \frac{4V_2}{\pi}\sin(\pi D_3)e^{i\frac{\pi}{2}} \tag{6}$$

$$V_{ij1} = \frac{4V_3}{\pi}\sin(\pi D_4)e^{i\frac{\pi}{2}} \tag{7}$$

Combing with (3)-(7), the voltage gain between the three ports can be obtained as:

$$\begin{cases} G_{12} = \dfrac{n_1 V_2}{n_2 V_1} == \dfrac{\sin(\pi D_1)\cos(\pi D_2)}{\sin(\pi D_3)} \\ G_{13} = \dfrac{n_1 V_3}{n_3 V_1} == \dfrac{\sin(\pi D_1)\cos(\pi D_2)}{\sin(\pi D_4)} \\ G_{23} = \dfrac{n_2 V_3}{n_3 V_2} == \dfrac{\sin(\pi D_3)}{\sin(\pi D_4)} \end{cases} \tag{8}$$

Where G_{12}, G_{13}, and G_{23} are the voltage gains between port 1 and port 2, port 1 and port3, port 2 and port 3. According to (8), it can be seen that the voltage gains between the three ports are decided by the duty cycles and independent of the load. Besides, four degrees of control freedom including D_1, D_2 in port 1 and D_3, D_4 in port 2, port 3 can be utilized to regulate the voltage gain. It should be mentioned the results can be also applied to other operation modes thanks to the same operation principle, such as SIDO mode while Port 2 is the input port, Port 1 and 3 are the output ports.

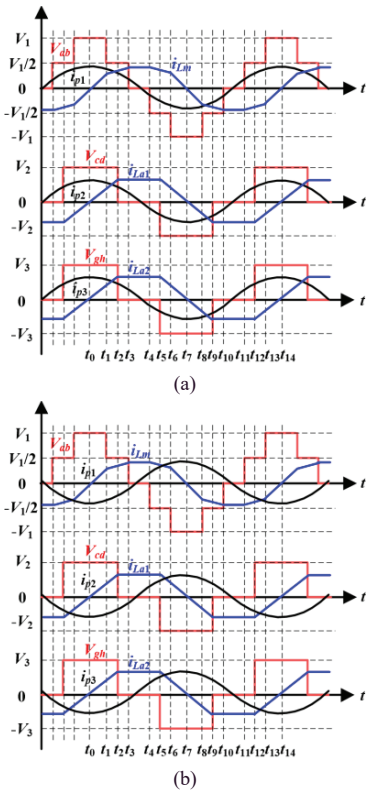

Fig. 4 The main operation waveforms of the proposed converter. (a) SIDO mode. (b) DISO mode.

TABLE I
LENGTH OF EACH STAGE IN HALF SWITCHING PERIOD

	Length
t_1	$0.5\cdot(D_1\text{-}D_2)\cdot T_s$
t_2	$0.5\cdot D_3\cdot T_s$
t_3	$0.5\cdot(D_1+D_2)\cdot T_s$
t_4	$0.5\cdot(1\text{-}D_1\text{-}D_2)\cdot T_s$
t_5	$0.5\cdot(1\text{-}D_3)\cdot T_s$
t_6	$0.5\cdot(1\text{-}D_1+D_2)\cdot T_s$
t_7	$0.5\cdot T_s$

B. ZVS Performance

The feasibility of achieving ZVS for the power switch is determined by the polarity of the sum of the resonant current plus the current through the auxiliary inductor or magnetic inductor when the power switch is turned on, neglecting the charging and discharging of junction capacitors and the deadtime. Based on this basic principle, the current constraints of ZVS realization are summarized in Table II according to Fig. 4. It should be mentioned that the ZVS constraints of the power switches in Port 2 and Port 3 are the same due to the same operation principles, which are not repeated here.

In Table II, it can be found that the current constraints of ZVS realization for each power switch are different due to the asynchronous switching, though the midpoint voltages of each port are synchronous. The expressions of i_{Lm} and i_{La1} can be calculated according to the voltages on L_m and L_{a1} during each working stage, while i_{p1} and i_{p2} are assumed as sine waves if ignoring the high order harmonics. Take S_1 as an example, $i_{p1}(t_{13})$ and $i_{Lm}(t_{13})$ are the resonant current and the current through the magnetic inductor when S_3 is turned off at t_{13}, which can be expressed as

$$\begin{cases} i_{p1}(t_{13}) = I_{p1}\sin(\pi\dfrac{1-2D_1+2D_2}{4}) \\ i_{Lm}(t_{13}) = -\dfrac{(D_1-D_2)V_1}{2f_sL_m} \end{cases} \tag{9}$$

Where I_{p1} is the amplitude of i_{p1} which can be expressed as [13]

$$I_{p1} = \frac{\pi P_1}{2V_1\sin(\pi D_1)\cos(\pi D_2)} \tag{10}$$

Where P_1 is the transferred power in Port 1. With the similar derivation method, the expressions of other currents in Table II can be obtained, thus the ZVS constraints of the proposed converter can be further derived and summarized in Table III. I_{p2} is the amplitude of i_{p2} which can be expressed as

$$I_{p1} = \frac{\pi P_2}{2V_2\sin(\pi D_3)} \tag{11}$$

As mentioned above, the operation principles of SIDO mode and DISO mode for the proposed converter are the same except that the resonant currents of each port are reversed, thus, different ZVS constraints are needed for the power switches of each port operating as input port and output port. Similarly, take S_1 for example, $i_{p1}(t_{13})$ is positive when Port 1 operates as input port and not satisfy the ZVS constraint of S_1, but $i_{Lm}(t_{13})$ is negative, which helps to achieve the ZVS of S_1. However, $i_{p1}(t_{13})$ and $i_{Lm}(t_{13})$ are both negative when Port 1 operates as output port, thus achieving the ZVS of S_1 more easily. With the similar method, the cases of other power switches when the corresponding port operates as input and output port can be obtained.

C. Comparision

To make better comparison with the existing 2L TPC and proposed converter, the topology and operation principle of 2L TPC under PWM method with FHS-PWM are added in Appendix. The main comparison results including the power switches and voltage gain are given as Table IV.

According to Table IV, it can be found 1) though the total amount of power switches of the proposed converter is more than that of the 2L TPC, power switches with only half of the voltage stress are needed in the Port 1 connected with MVDC, which is more beneficial for interfacing between the MVDC and LVDC grid; 2) one more degree of control freedom can be obtained in the proposed converter which makes the proposed converter has more wide range of operation voltage gain; 3) the characteristic that the voltage gain is independent of transferred power can also be achieved for the proposed converter

TABLE II

CURRENT CONSTRAINTS OF ZVS ACHIEVEMENT

S_1	S_2	S_3	S_4	S_5	S_6
$i_{p1}(t_{13})+i_{Lm}(t_{13})<0$	$i_{p1}(t_{10})+i_{Lm}(t_{10})<0$	$i_{p1}(t_3)+i_{Lm}(t_3)>0$	$i_{p1}(t_6)+i_{Lm}(t_6)>0$	$i_{p1}(t_4)+i_{Lm}(t_4)>0$	$i_{p1}(t_1)+i_{Lm}(t_1)>0$
S_7	S_8	S_9	S_{10}	S_{11}	S_{12}
$i_{p1}(t_8)+i_{Lm}(t_8)<0$	$i_{p1}(t_{11})+i_{Lm}(t_{11})<0$	$i_{p2}(t_{12})+i_{La1}(t_{12})>0$	$i_{p2}(t_2)+i_{La1}(t_2)<0$	$i_{p2}(t_5)+i_{La1}(t_5)<0$	$i_{p2}(t_9)+i_{La1}(t_9)>0$

TABLE III

FURTHER DERIVATION OF THE CURRENT CONSTRAINTS OF ZVS ACHIEVEMENT

S_1	S_2	S_3
$I_{p1}\sin(\pi\frac{1-2D_1+2D_2}{4})-\frac{(D_1-D_2)V_1}{2f_sL_m}<0$	$I_{p1}\sin(\pi\frac{3+2D_1+2D_2}{4})-\frac{D_1V_1}{2f_sL_m}<0$	$I_{p1}\sin(\pi\frac{1+2D_1+2D_2}{4})+\frac{D_1V_1}{2f_sL_m}<0$
S_4	S_5	S_6
$I_{p1}\sin(\pi\frac{3-2D_1+2D_2}{4})+\frac{(D_1-D_2)V_1}{2f_sL_m}<0$	$I_{p1}\sin(\pi\frac{3-2D_1-2D_2}{4})+\frac{D_1V_1}{2f_sL_m}<0$	$I_{p1}\sin(\pi\frac{1+2D_1-2D_2}{4})+\frac{(D_1-D_2)V_1}{2f_sL_m}<0$
S_7	S_8	S_9
$I_{p1}\sin(\pi\frac{3-2D_1+2D_2}{4})-\frac{(D_1-D_2)V_1}{2f_sL_m}<0$	$I_{p1}\sin(\pi\frac{1-2D_1-2D_2}{4})-\frac{D_1V_1}{2f_sL_m}<0$	$I_{p2}\sin(\pi\frac{1-2D_3}{4})-\frac{D_3V_2}{2f_sL_{a1}}<0$
S_{10}	S_{11}	S_{12}
$I_{p2}\sin(\pi\frac{1+2D_3}{4})+\frac{D_1V_1}{2f_sL_m}<0$	$I_{p2}\sin(\pi\frac{3-2D_3}{4})+\frac{D_3V_2}{2f_sL_{a1}}<0$	$I_{p2}\sin(\pi\frac{3+2D_3}{4})-\frac{D_3V_2}{2f_sL_{a1}}<0$

TABLE IV

COMPARISON RESULTS OF TWO-LEVEL TPC AND PROPOSED HYBRID-BRIDGE BASED TPC

items		Two-level TPC	Proposed Hybridge-based converter
Power switch	V_1	4	0
	$0.5\cdot V_1$	0	8
	total	12	16
Voltage gain	G_{12}	$\sin(\pi D_2)/\sin(\pi D_1)$	$\sin(\pi D_1)\cdot\cos(\pi D_2)/\sin(\pi D_3)$
	G_{13}	$\sin(\pi D_3)/\sin(\pi D_1)$	$\sin(\pi D_1)\cdot\cos(\pi D_2)/\sin(\pi D_4)$
	G_{23}	$\sin(\pi D_3)/\sin(\pi D_2)$	$\sin(\pi D_3)/\sin(\pi D_4)$
	Degree of control freedom	3	4
Independent of transferred power		Yes	Yes

IV. Simulation Verification

In order to verify the proposed converter, a 4-kW simulation model in PLECS is used, whereas the circuit parameters are shown in Table V. When the proposed converter operates in SIDO mode, Port 1 is utilized as an input port connected with a voltage source. Port 2 and Port 3 are utilized as output ports connected with resistor load. When the proposed converter operates in DISO mode, Port 1 is utilized as an output port connected with resistor load. Port 2 and Port 3 are utilized as input ports connected with two voltage sources.

TABLE V
Circuit Parameters of Proposed Converter in Simulation Mode

Item	Parameter
Voltage of port 1 V_1 (V)	400
Voltage of port 2 V_2 (V)	180~220
Voltage of port 3 V_3 (V)	180~220
Resonant capacitor C_r (μF)	50
Resonant inductor L_r (μH)	200
Magnetizing inductor L_m (μH)	400
Auxiliary inductors L_{a1}, L_{a2} (μH)	100
Turns ratio of the transformer n	2:1:1
Switching frequency (kHz)	50

Figs. 5(a)-(d) show the operation waveforms of the proposed converter working in SIDO mode with different work conditions. Fig. 5(e) shows the operation waveforms of the proposed converter working in DISO mode. In Figs. 5(a)-(e), the duty cycles and voltage of Port 1 are the same, namely, D_1=0.24, D_2=0.08, V_1=400V. The other parameters under different conditions are summarized in Table VI.

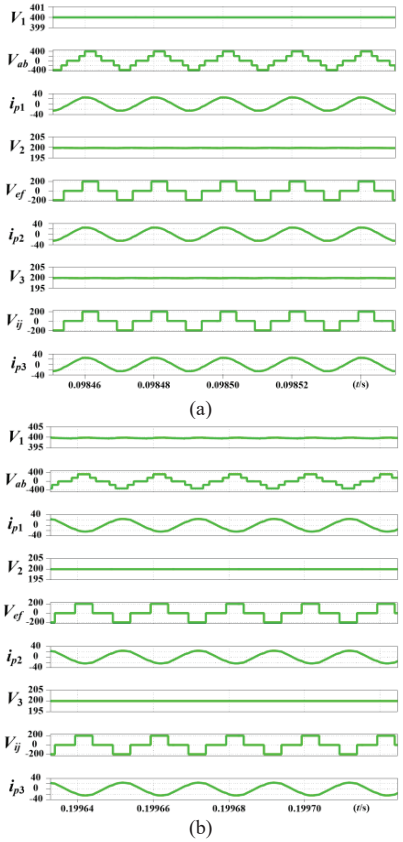

(a)

(b)

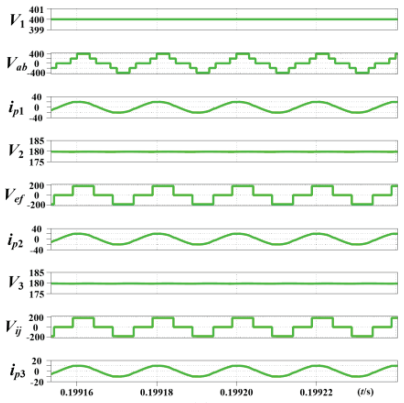

(c)

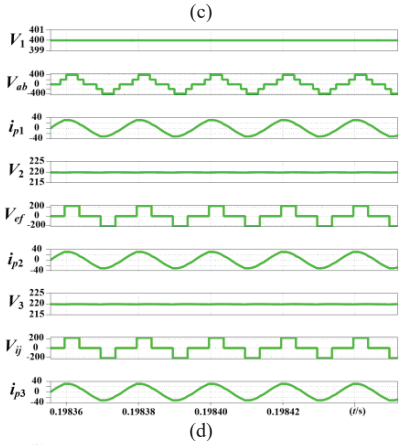

(d)

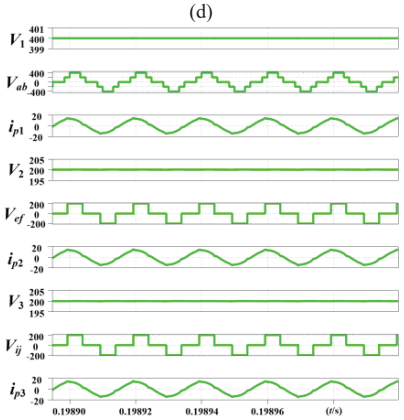

(e)

Fig. 5 Simulation results of proposed converter with corresponding modulation strategy. (a) SIDO mode V_2=V_3=200 V, P_{12}=P_{13}=2 kW. (b) DISO mode P_{21}=P_{31}=2 kW. (c) SIDO mode V_2=V_3=180 V. (d) SIDO mode V_2=V_3=220 V. (e) SIDO mode P_{12}=P_{13}=1 kW.

Comparing with Figs. 5(a) and (b), it can be seen that the duty cycles D_1-D_4 are the same in SIDO and DISO mode for the proposed converter, which means the operation principles of the proposed converter are the same and the direction of delivering power is only determined by the reference. From Figs. 5(a), (c), and (d), it can be seen that voltages of Port 2 and Port 3 can be adjusted from 180V to 220 V, which verifies that the performance of wide range of voltage gain for the proposed converter with the corresponding modulation strategy. From Figs. 5(a) and (e), it can be seen that the change of the resistive load from Port 2 and 3 has no effect on the voltage gain between each port, which means the voltage gain is decoupled with the load. The simulation results of the proposed converter are consistent with above theoretical analysis.

TABLE IV
PARAMETERS UNDER DIFFERENT CONDITIONS IN FIG. 5

Item	Parameters				
	Fig. 5(a)	Fig. 5(b)	Fig. 5(c)	Fig. 5(d)	Fig. 5(e)
Duty cycles of Port 2 and 3 D_3, D_4	0.23	0.23	0.26	0.2	0.23
Load of Port 2 and 3 R_2, R_3 (Ω)	20		20	20	40
Voltages of Port 2 and 3 V_2, V_3 (V)	200	200	180	220	200
Load of Port 1 R_1 (Ω)		40			
Delivering power between each port P_{12}, P_{13} (kW)	2	2	1.62	2.42	1

V. CONCLUSION

In this paper, a novel three-port hybrid bridge based bidirectional series-resonant converter with a corresponding modulation strategy is proposed. The proposed converter has following main merits: 1) hybrid-bridge structure is utilized which is more beneficial for interfacing MVDC and LVDC; 2) ZVS of all the switches can be achieved within the entire operation range with the help of auxiliary inductor; 3) wide range of operation voltage gain can be obtained thanks to four degrees of control freedom; 4) the voltage gain is independent of load. The simulation results are demonstrated to verify the effectiveness of the proposed converter.

APPENDEX

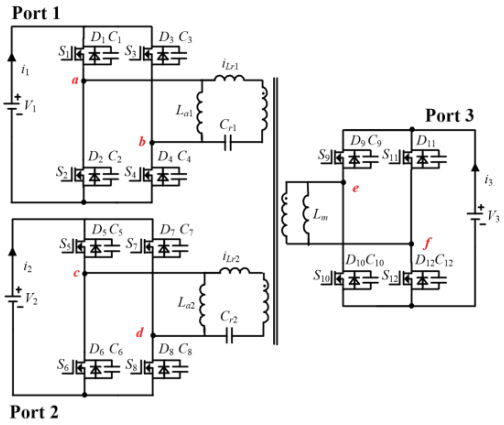

Fig. 6 Topology of 2L TPC

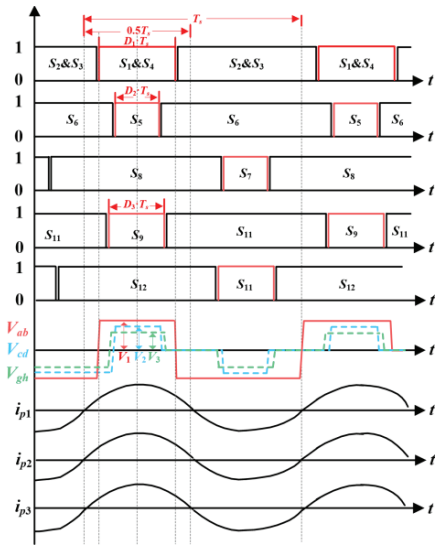

Fig. 7 Operation principle of PWM control with synchronized fist harmonic for two-level TPC.

REFERENCES

[1] Tomas K," Advances in Bidirectional DC-DC Converters for Future Energy Systems," Technical University of Denmark, 2018

[2] T. Dragiˇcevi´c, J. C. Vasquez, J. M. Guerrero, and D. ˇSkrlec, "Advanced LVDC electrical power architectures and microgrids: A step toward a new generation of power distribution networks," IEEE Electrification Magazine., vol. 2, no. 1, pp. 54–65, 2014.

[3] H. Ahmad, M. Hagiwara, "A compact high-power noninverting bidirectional buck–boost chopper for onboard battery energy storage systems," IEEE Trans. Power Electronics., Vol. 37, no. 2, pp. 1722-1735, Feb. 2022.

[4] T. Jiang, Q. Lin, J. Zhang and Y. Wang, "A novel ZVS and ZCS resonant converter for renewable energy systems," in Proc. IEEE Energy Convers. Congr. and Expo., Pittsburgh, PA, 2014, pp. 2296-2302.

[5] J. Zhang, H.Wu, X. Qin, and Y. Xing, "PWM plus secondary-side phaseshift controlled soft-switching full-bridge three-port converter for renewable power systems," IEEE Trans. Ind. Electron., vol. 62, no. 11, pp. 7061– 7072, Nov. 2015.

[6] H. Alijarajreh, D. Lu, Y. Siwakoti, and C. Tse, "A nonisolated three-port DC–DC converter with two bidirectional ports and fewer components," IEEE Trans. Power. Electronics., vol. 37, no. 7, pp. 8207– 8216, Jul. 2022.

[7] M. N. Kheraluwala, R. W. Gascoigne, D. M. Divan, and E. D. Baumann, "Performance characterization of a high-power dual active bridge DC-to-DC converter," IEEE Trans. Ind. Appl., vol. 28, no. 6, pp. 1294–1301, Nov./Dec. 1992.

[8] E. S. Oluwasogo, and H. Cha, "Self-current sharing in dual-transformer-based triple-port active bridge DC–DC converter with reduced device count," IEEE Trans. Power Electronics., vol. 36, no. 5, pp. 5290–5301, May. 2021.

[9] T. Jiang, Q. Lin, J. Zhang and Y. Wang, "A novel two-phase interleaved LLC series-resonant converter for renewable energy systems," in Proc. IEEE Energy Convers. Congr. and Expo., Pittsburgh, PA, 2014, pp. 2296- 2302.

[10] J. Wu. X. Yan, X. Sun, X. Su, H. Du, and X. Wang, "A series resonant three-port DC–DC converter with decoupling function and magnetic integration," IEEE Trans. Power Electronics., vol. 37, no. 12, pp. 14720– 14737, Jul. 2022.

[11] H. Wu, K. Sun, Y. Li and Y. Xing, "Fixed-Frequency PWM-Controlled Bidirectional Current-Fed Soft-Switching Series-Resonant Converter for Energy Storage Applications," IEEE Trans. on Ind. Electron., vol. 64, no. 8, pp. 6190-6201, Aug. 2017.

[12] H. Wu, S. Ding, K. Sun, L. Zhang, Y. Li and Y. Xing, "Bidirectional soft-switching series-resonant converter with simple PWM control and load-independent voltage-gain characteristics for energy storage system in DC microgrids," IEEE J. Emerg. Sel. Topics Power Electron., vol. 5, no. 3, pp. 995-1007, Sept. 2017.

[13] X. Tang, H. Wu, W. Hua and Y. Xing, "Three-port bidirectional series-resonant converter with first-harmonic-synchronized PWM," IEEE J. Emerg. Sel. Topics Power Electron., vol. 9, no. 2, pp. 1410-1420, April. 2021.

[14] Sabate J A, Lee F C Y. Offline application of the fixed-frequency clamped-mode series resonant converter[J]. IEEE Transactions on Power Electronics, 1991, 6(1): 39-47.

[15] P. Liu, C. Chen, and S. Duan, "An optimized modulation strategy for the three-level DAB converter with five control degrees of freedom," *IEEE Trans. Ind. Electron.,* vol. 67, no. 1, pp. 254–264, Jan. 2022.